Distribution of normalized water-leaving radiances at UV and visible wave bands in relation with chlorophyll a and colored detrital matter content in the southeast Pacific

Marc Tedetti, Bruno Charrière, Annick Bricaud, Julien Para, Patrick Raimbault, Richard Sempere

JOURNAL OF GEOPHYSICAL RESEARCH, VOL. 115, C02010, doi:10.1029/2009JC005289, 2010

Distribution of normalized water-leaving radiances at UV and visible wave bands in relation with chlorophyll *a* and colored detrital matter content in the southeast Pacific

Marc Tedetti,[1] Bruno Charrière,[1] Annick Bricaud,[2] Julien Para,[1] Patrick Raimbault,[1] and Richard Sempéré[1]

Received 19 January 2009; revised 15 May 2009; accepted 18 September 2009; published 12 February 2010.

$nL_w(\lambda)$ (μW cm^{-2} sr^{-1}) were recorded in the hyperoligotrophic waters of the South Pacific Gyre, with values increasing with wavelength from 305 (nL_w = 0.64) to 380 nm (nL_w = 3.18) in the UV range and decreasing from 412 (nL_w = 4.46) to 565 nm (nL_w = 0.23) in the visible region. The intense $nL_w(\lambda)$ observed in the violet-blue domains were attributed to very low absorptions of colored detrital matter (CDM), likely related to a strong photobleaching of colored dissolved organic matter in the surface waters. We evaluated the relationships between the UV, violet, or blue/green wave band ratios of $nL_w(\lambda)$ and surface total chlorophyll *a* (TChl *a*) concentration and CDM absorption ($a_{CDM}(\lambda)$). For TChl *a*, the best correlation was found with the blue/green ratio at 443 nm: TChl *a* (mg m^{-3}) = 2.37$[nL_w(443)/nL_w(565)]^{-1.51}$ (r^2 = 0.86 and RMS error (RMSE) = 23%). By contrast, for $a_{CDM}(\lambda)$, the best correlation was observed when using the UV/green ratio at 325 nm: $a_{CDM}(325)$ (m^{-1}) = 0.16$[nL_w(325)/nL_w(565)]^{-0.69}$ (r^2 = 0.82 and RMSE = 16%). These results show the potential role of $nL_w(\lambda)$ at UV wave bands for the assessment, through empirical algorithms, of colored detrital matter in the surface oceanic waters.

Citation: Tedetti, M., B. Charrière, A. Bricaud, J. Para, P. Raimbault, and R. Sempéré (2010), Distribution of normalized water-leaving radiances at UV and visible wave bands in relation with chlorophyll *a* and colored detrital matter content in the southeast Pacific, *J. Geophys. Res.*, *115*, C02010, doi:10.1029/2009JC005289.

1. Introduction

[2] Normalized water-leaving radiance ($nL_w(\lambda)$ in μW cm^{-2} sr^{-1}, where λ refers to wavelength in nm) is defined as the radiance that would emerge from the ocean in the absence of atmosphere, with the Sun at zenith, at the mean Earth-Sun distance [*Gordon and Clark*, 1981; *Gordon*, 2005]. Belonging to apparent optical properties (AOPs), $nL_w(\lambda)$ is dependent on both inherent optical properties (IOPs) and the light field in which it is measured. Conversely, IOPs, which include, among others, absorption ($a(\lambda)$ in m^{-1}) and backscattering ($b_b(\lambda)$ in m^{-1}) coefficients, are controlled only by the concentrations of optically active components present in seawater [*Preisendorfer*, 1961; *Kirk*, 1994]. Together with remote sensing reflectance ($R_{rs}(\lambda)$ in sr^{-1}) and irradiance reflectance ($R(\lambda)$, dimensionless), $nL_w(\lambda)$ is the (derived) quantity specifically used in ocean color studies. Since they are proportional to $b_b(\lambda)$ and inversely proportional to $a(\lambda)$, $nL_w(\lambda)$, $R_{rs}(\lambda)$, and $R(\lambda)$ have been utilized, mainly in the visible spectral domain (400–700 nm), to retrieve the concentrations of some marine biogeochemical constituents [*Morel and Prieur*, 1977; *Gordon et al.*, 1988].

[3] Many studies have reported empirical or semianalytical algorithms linking the violet (412 nm) or blue (443 or 490 nm)/green (555 or 560 nm) wave band ratios of $nL_w(\lambda)$ or $R_{rs}(\lambda)$ to surface chlorophyll *a* (Chl *a*) concentration (mg m^{-3}) [*Gordon et al.*, 1988; *O'Reilly et al.*, 2000; *D'Ortenzio et al.*, 2002; *Garcia et al.*, 2005]. In recent years, important efforts have been made to extract other biogeochemical elements of interest from ocean color data. For instance, *Uitz et al.* [2006] performed an empirical parameterization to derive the vertical distribution of different phytoplankton groups (microplankton, nanoplankton, and picoplankton). Algorithms have also been elaborated for estimating surface particulate organic carbon (POC) concentration (mg m^{-3}) from the $R_{rs}(443)/R_{rs}(555)$ or

[1] Laboratoire de Microbiologie, Géochimie et Ecologie Marines, Centre d'Océanologie de Marseille, Université de la Méditerranée, INSU, CNRS, Marseille, France.
[2] Laboratoire d'Océanographie de Villefranche, Université Pierre et Marie Curie-Paris 6, INSU, CNRS, Villefranche-sur-Mer, France.

0148-0227/10/2009JC005289$09.00

$R_{rs}(490)/R_{rs}(555)$ ratios [*Stramski et al.*, 1999; *Pabi and Arrigo*, 2006; *Stramski et al.*, 2008]. Moreover, several works have focused on the appraisal of surface colored detrital matter (CDM), i.e., the material that efficiently absorbs light over a broad range of ultraviolet (UV) (280–400 nm) and, to a lesser extent, visible wavelengths. CDM is composed at ~90% by colored dissolved organic matter (CDOM; also known as gelbstoff, gilvin, or yellow substances) and at ~10% by nonalgal particulate matter (NAP; comprising detritus and heterotrophic organisms) [*Siegel et al.*, 2002], whose absorption spectra both increase monotonically with decreasing wavelength [*Bricaud et al.*, 1981; *Nelson et al.*, 1998]. CDM absorption has been mainly computed at 443 nm ($a_{\mathrm{CDM}}(443)$) using $nL_w(443)$ or $R_{rs}(443)$ measurements and semianalytical models [*Siegel et al.*, 2002; *Maritorena and Siegel*, 2005; *Ciotti and Bricaud*, 2006].

[4] Recently, the optical and biogeochemical properties of the southeast Pacific have been investigated in the frame of the Biogeochemistry and Optics South Pacific Experiment (BIOSOPE) cruise [*Claustre et al.*, 2008]. The southeast Pacific waters, as open ocean waters away from the influence of terrestrial inputs, are case 1 waters, i.e., waters in which the bulk optical properties may be derived solely from phytoplankton concentration [*Morel and Prieur*, 1977]. Bio-optical data acquired during the BIOSOPE campaign confirmed (remote sensing data had already pointed it out [*Claustre and Maritorena*, 2003]) that the center of the South Pacific Gyre (SPG), near Easter Island, contains the clearest and the most oligotrophic known oceanic waters [*Morel et al.*, 2007a; *Tedetti et al.*, 2007; *Twardowski et al.*, 2007]. Interestingly, *Morel et al.* [2007b] compared the bio-optical properties within the visible and UV spectral domains of two case 1 water bodies: the southeast Pacific and the Mediterranean Sea. These authors observed, for similar Chl *a* concentrations, relatively high differences between the SPG and the Mediterranean Sea in the $R(\lambda)$ and diffuse attenuation coefficient for downward irradiance ($K_d(\lambda)$ in m^{-1}) values of the UV range, while these differences substantially decreased or tended to disappear toward the visible domain. Actually, for the same Chl *a* content, R(UV) were systematically higher and K_d(UV) were systemically lower in the southeast Pacific compared to the Mediterranean waters. Because CDM (or CDOM) drive the bio-optical properties of the UV region, it has been suggested that phytoplankton biomass and colored material content could exhibit different degrees of coupling within case 1 waters [*Morel et al.*, 2007b].

[5] Consequently, for a complete characterization of bio-optical properties of an oceanic province, it appears that visible but also UV ocean color data are necessary. However, in situ measurements of AOPs, especially $nL_w(\lambda)$ and $R_{rs}(\lambda)$, in the UV range are still scarce, in part because direct applications to remote sensing are not possible. In this particular area of the southeast Pacific, although $R(\lambda)$ and $K_d(\lambda)$ data have been provided in the whole UV domain (spectrally or at several discrete wavelengths from 300 to 400 nm) [*Morel et al.*, 2007a, 2007b; *Tedetti et al.*, 2007], $R_{rs}(\lambda)$ values were described merely from 380 nm [*Stramski et al.*, 2008]. In addition, to our knowledge, no data concerning the relationships between nL_w(UV) or R_{rs}(UV) and biogeochemical parameters such as Chl *a* or CDM are currently available.

[6] The first objective of the present study is to investigate the distribution of $nL_w(\lambda)$ at several UV (from 305 to 380 nm) and visible (from 412 to 565 nm) wave bands in different contrasted areas of the southeast Pacific, including the hyperoligotrophic SPG and coastal waters. The second aim is to examine the relationships between $nL_w(\lambda)$ and Chl *a* concentration and CDM absorption measured on discrete samples in the surface waters. The comparison of these relationships within the UV and visible ranges will allow the estimation of divergences between these two spectral domains in the empirical algorithms relating AOPs and IOPs.

2. Material and Methods

2.1. Study Area

[7] Field measurements were carried out during the BIOSOPE cruise aboard R/V *l'Atalante* from 26 October to 11 December 2004. Twenty-one stations were sampled along a 8000 km west to east transect between the Marquesas Islands (8°S, 141°W) and the coast of Chile (34°S, 72°W) (Figure 1 and Table 1). This transect encompassed several oceanic areas with different trophic conditions, such as the mesotrophic subequatorial waters near the Marquesas Islands, the hyperoligotrophic waters of the SPG (20°S–30°S, 98°W–123°W), and the eutrophic waters associated with upwelling of Chile. General biogeochemical and physical characteristics of these oceanic provinces are described by *Claustre et al.* [2008]. Two types of stations were studied: the "short" (8 h) stations (STB and STA) and the "long" stations, investigated over 2–5 days. The latter included the Marquesas Islands (MAR), the high-nutrients low-chlorophyll zone (HNL), the center of the SPG (GYR), east of the SPG (EGY), and upwelling of Chile (UPW and UPX). The SPG comprised the stations STB5, STB6, STB7, GYR, STB11, and STB12 (Figure 1 and Table 1). The positions of four of these long stations were determined from Sea-viewing Wide Field-of-view Sensor (SeaWiFS), Moderate Resolution Imaging Spectroradiometer (MODIS Aqua), and Medium-Resolution Imaging Spectrometer (MERIS) real-time ocean color data to sample the lowest (GYR) and the highest (MAR, UPW, and UPX) surface Chl *a* concentrations (Figure 1).

2.2. In Situ Radiometric Measurements

[8] Two profiles of upward radiance ($L_u(Z, \lambda)$ in $\mu W\ cm^{-2}\ sr^{-1}$) and downward irradiance ($E_d(Z, \lambda)$ in $\mu W\ cm^{-2}$) were made at each station (Figure 1) close to solar noon using a MicroPro free-fall profiler (Satlantic, Inc.) equipped with OCR-504 upward radiance and downward irradiance sensors in the UV (305, 325, 340, and 380 nm) and visible (412, 443, 490, and 565 nm) spectral domains. Surface irradiance ($E_s(\lambda)$ in $\mu W\ cm^{-2}$), which is equivalent to the downward irradiance just above the sea surface ($E_d(0^+, \lambda)$), was simultaneously measured at the same wave bands on the ship deck using OCR-504 downward irradiance sensors (surface reference). For in-water sensors, the full width at half maximum (FWHM) of the wave bands was 2 nm for 305, 325, and 340 nm and 10 nm for 380, 412, 443, 490, and 565 nm. For in-air sensors, the FWHM was 2 nm for 305, 325, and 340 nm; 10 nm for 380 nm; and 20 nm for 412, 443, 490, and 565 nm. For the UV wave bands, the accuracy of the cosine response for downward irradiance within 0°–60° was 4%

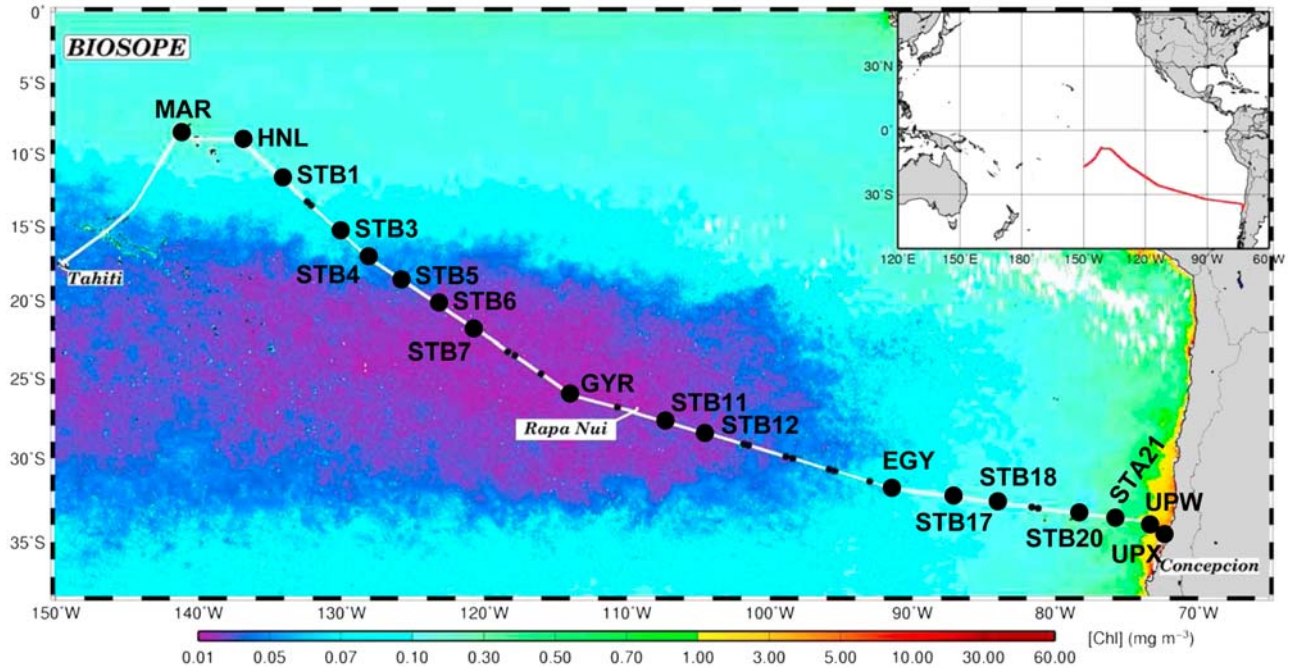

Figure 1. Map of the Biogeochemistry and Optics South Pacific Experiment (BIOSOPE) cruise track superimposed on a Sea-viewing Wide Field-of-view Sensor composite for November and December 2004 showing Chl *a* concentration in the upper layer. The stations studied include the Marquesas Islands (MAR), the high-nutrients low-chlorophyll zone (HNL), the center of the South Pacific Gyre (GYR), east of the South Pacific Gyre (EGY), and upwelling of Chile (UPW and UPX). STB and STA stations are "short" (8 h) stations, whereas MAR, HNL, GYR, EGY, UPW, and UPX are "long" stations, investigated over 2–5 days. The South Pacific Gyre comprises the stations STB5, STB6, STB7, GYR, STB11, and STB12. Rapa Nui is Easter Island.

and 8% for in-air and in-water sensors, respectively. For the visible wave bands, the accuracy of the cosine response for downward irradiance within 0°–60° was 3% for in-water and in-air sensors. The field of view of upward radiance sensors was 10° in water. All the sensors were calibrated just before the cruise by Satlantic, Inc.

[9] The MicroPro free-fall profiler, equipped with pressure, temperature, and tilt sensors, was operated from the

Table 1. Position and Date of the Stations Investigated During the BIOSOPE Cruise[a]

Station	Area	Position	Date
MAR2	Marquesas Islands	8.39°S, 141.27°W	27 Oct 2004
MAR4	Marquesas Islands	8.32°S, 141.27°W	29 Oct 2004
HNL2	High-nutrients low-chlorophyll zone	9.01°S, 136.89°W	1 Nov 2004
STB1		11.74°S, 134.10°W	3 Nov 2004
STB3		15.53°S, 129.93 °W	5 Nov 2004
STB4		17.23°S, 127.97°W	6 Nov 2004
STB5	South Pacific Gyre	18.75°S, 125.55°W	7 Nov 2004
STB6	South Pacific Gyre	20.45°S, 122.89°W	8 Nov 2004
STB7	South Pacific Gyre	22.05°S, 120.38°W	9 Nov 2004
GYR5	Center of South Pacific Gyre	26.06°S, 114.0°W	15 Nov 2004
STB11	South Pacific Gyre	27.77°S, 107.29°W	20 Nov 2004
STB12	South Pacific Gyre	28.54°S, 104.31°W	21 Nov 2004
EGY3	East of South Pacific Gyre	31.85°S, 91.44°W	27 Nov 2004
EGY4	East of South Pacific Gyre	31.86°S, 91.41°W	28 Nov 2004
EGY5	East of South Pacific Gyre	31.90°S, 91.41°W	29 Nov 2004
STB17		32.40°S, 86.78°W	1 Dec 2004
STB18		32.68°S, 84.07°W	2 Dec 2004
STB20		33.35°S, 78.12°W	4 Dec 2004
STA21		33.58°S, 75.84°W	5 Dec 2004
UPW1	Upwelling of Chile	34.00°S, 73.37°W	6 Dec 2004
UPX2	Upwelling of Chile	34.58°S, 72.43°W	10 Dec 2004

[a]For the radiometric measurements, HNL, GYR, UPW, and UPX were sampled for 1 day (day 2, 5, 1, and 2 referring to HNL2, GYR5, UPW1, and UPX2, respectively), whereas MAR and EGY were sampled for 2 and 3 days, respectively (day 2 and 4 referring to MAR2 and MAR4, respectively, and day 3, 4, and 5 referring to EGY3, EGY4, and EGY5, respectively). For Chl *a* concentration and CDM absorption measurements, sampling was conducted at each short station and each day of each long station. BIOSOPE, Biogeochemistry and Optics South Pacific Experiment.

rear and deployed ~30 m away to remove the shadowing effects and disturbances of the ship. Each cast was accompanied by a measurement of the dark current (instrument on the deck) and a pressure tare (instrument at sea surface). The operating depth of the profiler was 200 m, and its free-fall descent rate ranged from 0.5 to 0.8 m s^{-1}. The surface reference was set up at the top of the mast of the ship (~20 m above water) to avoid shadowing or reflecting obstacles. Measurements were logged using Satlantic's Satview 2.6 software, and data were prepared and processed using Satlantic's ProSoft 7.6 software. The latter allowed for initial data processing, such as the application of radiometric calibration, dark correction, immersion coefficient, pressure tare, and data interpolation (0.1 m depth resolution) and the removal of data with tilt >5°. Solar zenith angle at the time of the measurements ranged between 15° and 48°, with a mean value of 29° ± 9° for the whole transect.

2.3. Determination of $nL_w(\lambda)$

[10] Determination of $nL_w(\lambda)$ from in-water radiometry was conducted according to *Mueller et al.* [2003]. Diffuse attenuation coefficient for upward radiance ($K_L(\lambda)$ in m^{-1}) was calculated from the slope of the linear regression of the log-transformed upward radiance versus depth in accordance with the relationship

$$L_u(Z_2, \lambda) = L_u(Z_1, \lambda)e^{[-K_L(\lambda)(Z_2 - Z_1)]}, \quad (1)$$

where $L_u(Z_1, \lambda)$ and $L_u(Z_2, \lambda)$ are the upward radiances (μW cm^{-2} sr^{-1}) at depths Z_1 and Z_2 (m), respectively. The depth interval within the upper water column used for the $K_L(\lambda)$ determination was chosen from a visual examination of each log-transformed profile and was typically 5, 10, 15, 20, or 30 m, depending on the stations and wave bands. The determination coefficients (r^2) of the $K_L(\lambda)$ calculation were >0.98. Water-leaving radiance ($L_w(\lambda)$ in μW cm^{-2} sr^{-1}) was then derived from the relationship

$$L_w(\lambda) = \frac{t}{n^2} L_u(0^-, \lambda), \quad (2)$$

where $L_u(0^-, \lambda)$ is the upward radiance beneath the sea surface computed by extrapolating $L_u(Z, \lambda)$ to the sea surface from $K_L(\lambda)$ and equation (1), t (~0.975) is the upward Fresnel transmittance of the air-sea interface, and n (~1.34) is the refractive index of water. Normalized water-leaving radiance ($nL_w(\lambda)$ in μW cm^{-2} sr^{-1}) was determined by the formula [*Gordon and Clark*, 1981]

$$nL_w(\lambda) = \frac{L_w(\lambda)}{E_s(\lambda)} F_0(\lambda), \quad (3)$$

where $E_s(\lambda)$ is the surface irradiance and $F_0(\lambda)$ is the solar irradiance at the top of the atmosphere, at the mean Earth-Sun distance (μW cm^{-2}). $F_0(\lambda)$ data in the ranges 305–340 nm and 380–565 nm were used from *Thuillier et al.* [1997, 1998], respectively.

[11] The $nL_w(\lambda)$ data presented in this study are either average values based on the two upward radiance profiles (coefficient of variation <8% for all the stations concerned) or values based on one profile only, when the other profile was acquired under variable sky conditions (broken clouds) and thus rejected. This latter case involves the stations STB6, STB11, STB12, EGY3, EGY5, STB18, STA21, and UPW1. Moreover, $nL_w(\lambda)$ obtained in STB7 and STB20 were removed from the data set presented here because of some suspicious radiometric values.

2.4. TChl *a* Concentration Measurements

[12] Discrete water samples were collected at each station in surface waters (at 5–20 m depth) using a SeaBird Electronics 911plus conductivity-temperature-depth (CTD)–Carousel system, supporting twenty 12 L Niskin bottles equipped with Teflon rings to avoid carbon contaminations. Sampling for Chl *a* was performed on the 0900 LT CTD cast, whereas that for CDOM and NAP was done on the 1200 LT cast. For Chl *a*, 280 mL of seawater was filtered through 25 mm Whatman GF/F filters (nominal pore size around 0.7 μm) immediately after sampling and was placed in glass tubes containing 5 mL of pure methanol as described by *Raimbault et al.* [2004]. Following 20–30 min of extraction, fluorescence of the extract was determined on a Turner Fluorometer 110 equipped with the Welschmeyer kit to avoid chlorophyll *b* (Chl *b*) interference [*Welschmeyer*, 1994]. As the monochromatic fluorescence method cannot separate divinyl chlorophyll from chlorophyll, results are given in terms of total Chl *a* (TChl *a*) concentration (mg m^{-3}), i.e., the sum of Chl *a* and divinyl Chl *a* concentrations. The blank "methanol + filter" was close to zero, giving a very low detection limit of around 0.01 mg m^{-3}. Calibrations were made using a pure Sigma Chl *a* standard. For UPW1 station, surface TChl *a* concentration was not measured, so we used the TChl *a* value reported by *Ras et al.* [2008], who used the high-performance liquid chromatography (HPLC) method. In situ TChl *a* was assessed with an AQUA^{tracka} III fluorometer (Chelsea Technologies Group) attached on the CTD–Carousel system. Depth of TChl *a* maximum (DCM in m) was evaluated from in situ TChl *a* profiles.

2.5. CDOM and NAP Absorption Spectra Measurements

[13] Absorption coefficients of CDOM ($a_{CDOM}(\lambda)$ in m^{-1}) were measured throughout the UV-visible domain (280–735 nm) using the multiple path length, liquid core waveguide system UltraPath (World Precision Instruments, Inc.), with a path length of 2 m. Samples were filtered immediately after collection, in dim light, using 0.2 μm Millipore filters prerinsed with Milli-Q water. Filtered samples were then placed in the automatic sampler (maintained in the dark) and pumped into the sample cell of the Ultrapath instrument. Absorbance spectra were measured with reference to a salt solution (35 practical salinity units), prepared with HPLC-quality water and granular NaCl, to match the salinity and refractive index of samples. Between measurements, the cell was flushed successively with diluted detergent, high reagent grade methanol, 2 M HCl, and Milli-Q water, and the cleanliness of the tube was controlled using a reference value for the transmittance of the reference water. As the absorption coefficients of pure water vary with temperature (especially in the infrared), the temperature differences between reference and sample were minimized. The presence of microbubbles in the sample cell was also avoided by using a peristaltic pump and a debubbler. Surface $a_{CDOM}(\lambda)$

Table 2. In Situ Surface TChl *a* Concentration and Depth of TChl *a* Maximum[a]

Station	TChl *a* (mg m^{-3})	DCM (m)
MAR2	0.440	50
MAR4	0.320	60
HNL2	0.152	80
STB1	0.172	80
STB3	0.061	120
STB4	0.060	130
STB5	0.049	140
STB6	0.022	180
STB7	0.027	195
GYR5	0.029	180
STB11	0.042	190
STB12	0.029	180
EGY3	0.089	80
EGY4	0.084	80
EGY5	0.086	80
STB17	0.132	70
STB18	0.139	70
STB20	0.404	50
STA21	0.206	50
UPW1	1.300[b]	40
UPX2	0.972	20

[a]TChl *a*, total chlorophyll *a*; DCM, depth of TChl *a* maximum.
[b]Data from *Ras et al.* [2008].

values were not available at stations MAR2, STB6, STB11, STB12, and STB18.

[14] For particulate absorption measurements, seawater samples (with volumes varying from 1 L in the upwelling area to 11.2 L in the SPG) were collected on 25 mm Whatman GF/F filters, and absorption spectra were measured directly on the filters, by reference to a blank wet filter, with a Perkin-Elmer Lambda-19 spectrophotometer equipped with an integrating sphere. Spectra were acquired between 300 and 800 nm with a 2 nm step. For each sample, the contribution of NAP to total particulate absorption was determined by immersing the filter in methanol so as to extract pigments and measuring again the absorption spectrum [*Kishino et al.*, 1985]. All spectra were shifted to zero in the infrared by subtracting the average optical density between 750 and 800 nm. Finally, optical densities were corrected for the path length amplification effect using empirical algorithms derived by *Allali et al.* [1997] for oligotrophic and mesotrophic waters and by *Bricaud and Stramski* [1990] for eutrophic waters. They were then converted into absorption coefficients of total particulate and NAP ($a_P(\lambda)$ and $a_{NAP}(\lambda)$, respectively, in m^{-1}).

[15] In spite of the long extraction time (2 days), residual absorption by pigments was still present on numerous samples. To correct for this effect, $a_{NAP}(\lambda)$ were determined by fitting the actual spectra to an exponential function

$$a_{NAP}(\lambda) = a_{NAP}(\lambda_0)e^{[-S(\lambda-\lambda_0)]} \quad (4)$$

in the 300–380, 520–640, and 700–750 nm ranges, where the residual absorption by pigments can be assumed to be negligible. The spectral slope coefficient (S) values ranged from 0.007 to 0.014 nm^{-1}, with an average value of 0.0094 (±0.0018) nm^{-1}. Absorption coefficients of phytoplankton ($a_{Phy}(\lambda)$ in m^{-1}) were also computed by subtracting $a_{NAP}(\lambda)$ from $a_P(\lambda)$. Surface $a_{NAP}(\lambda)$ and $a_{Phy}(\lambda)$ values were not available at station STB12. Absorption coefficients of CDM ($a_{CDM}(\lambda)$ in m^{-1}) were determined as the sum of $a_{CDOM}(\lambda)$ and $a_{NAP}(\lambda)$ and are presented here at the same eight wave bands as $nL_w(\lambda)$.

2.6. Calculation of Root-Mean-Square Errors

[16] The performance of power functions linking $nL_w(\lambda)$ and biogeochemical parameters was quantified by calculating root-mean-square errors (RMSEs) between retrieved and measured TChl *a* concentration or $a_{CDM}(\lambda)$ values. RMSEs were computed as relative values (expressed in %) to give equal weights to all measurements.

3. Results and Discussion

3.1. Hydrological Characteristics

[17] The general distributions of temperature and salinity are presented and described by *Claustre et al.* [2008]. Concisely, surface temperature decreased from west to east with 27.6°C in the Marquesas Islands (MAR2 and MAR4) and ~15°C in upwelling of Chile (UPW1 and UPX2). In the SPG, surface temperature ranged from 21°C (STB12) to 26°C (STB5), whereas in its eastern border (EGY), surface temperature was 18.7°C. Surface salinity showed the same pattern with higher values westward (35.75 in MAR2 and MAR4) and lower values eastward (34.25 in UPW1 and UPX2). A maximum of 36.5 was recorded around 130°W (STB3 and STB4).

3.2. TChl *a* Concentrations

[18] In situ surface TChl *a* concentrations, in accordance with ocean color data, displayed large variations in the southeast Pacific (Table 2). The highest surface TChl *a* concentrations were found at the two extremities of the transect: ~0.40 and 1.00 mg m^{-3} in the Marquesas Islands and upwelling of Chile, respectively. In the Marquesas Islands, surface TChl *a* concentrations were higher than those previously observed in this subequatorial area at other periods of the year [*Signorini et al.*, 1999]. This could be explained by the vertical inputs of dissolved iron from subsurface waters leading to an enhancement of phytoplankton growth [*Blain et al.*, 2008]. From October to March, wind-driven coastal upwelling fertilizes the surface waters off Chile, leading to one of the most productive zones of the global ocean [*Carr*, 2001]. The lowest surface TChl *a* concentrations were observed in the SPG: 0.022, 0.027, and 0.029 mg m^{-3} in STB6, STB7, and GY5, respectively (Table 2). These very low values confirm the hyperoligotrophic status of the SPG. In this area, primary production was strongly nutrient-limited because of the absence of terrestrial inputs and the depth of the nutricline (0.01 μM N at ~160 m) [*Raimbault et al.*, 2008]. Our TChl *a* concentrations are in good agreement with those measured with the HPLC technique by *Ras et al.* [2008]. Since these authors measured TChl *a* from the 1200 LT CTD cast (which is the cast of our CDOM and NAP sampling), this good agreement confirms that the time lag (~3 h) between our TChl *a* and CDOM and NAP sampling has no influence on the relationships described in section 3.4. The DCM depth revealed considerable differences along the transect (Table 2). It increased from the Marquesas Islands (~55 m) to the SPG, with the highest value observed in STB7 (195 m), and substantially decreased from the SPG toward the upwell-

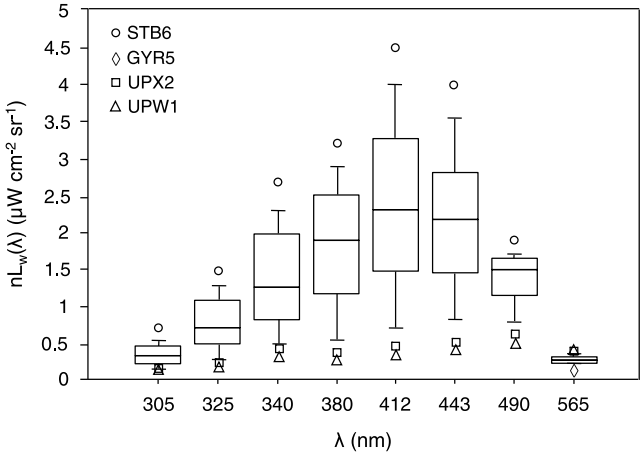

Figure 2. Box-and-whisker plots for the distribution of normalized water-leaving radiances ($nL_w(\lambda)$) in the UV (305, 325, 340, and 380 nm) and visible (412, 443, 490, and 565 nm) spectral domains along the transect. The bottom and top of the boxes are the 25th and 75th percentiles, respectively, whereas the central line is the 50th percentile (the median). The ends of the error bars or "whiskers" correspond to the 10th percentile (bottom) and to the 90th percentile (top). The different dots represent the observations <10th percentile and the observations >90th percentile. For all the wave bands, with the exception of the green one, $nL_w(\lambda)$ at STB6 was higher than the 90th percentile, and $nL_w(\lambda)$ at UPX2 and UPW1 were lower than the 10th percentile. For the green wave band, we observed the inverse pattern with $nL_w(\lambda)$ at UPX2 and UPW1 being >90th percentile and $nL_w(\lambda)$ at GYR5 being <10th percentile. No outliers were present in this distribution.

ing area of Chile to reach 20 m in UPX2. In the Marquesas Islands and east of 110°W, the DCM was generally located just above the depth of the euphotic zone (Z_e; depth of 1% of the surface photosynthetically available radiation), whereas in the SPG it was always found below Z_e [*Raimbault et al.*, 2008].

3.3. Distribution of $nL_w(\lambda)$ Across the Southeast Pacific

[19] Across the southeast Pacific, $nL_w(\lambda)$ presented great variations (Figure 2). Values increased from the Marquesas Islands to the SPG and diminished from the SPG to upwelling of Chile. The station exhibiting the highest $nL_w(\lambda)$ in the UV (305–380 nm), violet (412 nm), and blue (443 and 490 nm) ranges was STB6, followed by GYR5 and STB12, which displayed very similar values. By contrast, the station revealing the lowest UV, violet, and blue $nL_w(\lambda)$, and at the same time the highest $nL_w(565)$, was UPW1 followed by UPX2, in the coastal waters off Chile. For most of the stations, $nL_w(\lambda)$ increased from the shortest UV wave band to the violet domain, where it reached its maximal value and then decreased in the direction of blue and green wave bands (Figure 2). It appeared that $nL_w(305)$ was higher than $nL_w(565)$ only in the clearest stations: STB1–STB6, GYR5, STB11, and STB12.

[20] Other authors reported ocean color data in the southeast Pacific in the frame of the BIOSOPE program. By using a LI-COR spectroradiometer (LI-1800 UW), *Morel et al.* [2007a, 2007b] measured downward and upward spectral irradiances from which they determined $R(\lambda)$ beneath the surface in the whole UV and visible domains. In the SPG, they observed that maximal $R(\lambda)$ values were slightly higher than 13% in the near UV domain (at ~394 nm) and that $R(310)$ values were as high as 6%. *Stramski et al.* [2008] evaluated $R_{rs}(\lambda)$ in the range 380–800 nm from subsurface (0.2 m depth) measurements of $L_u(\lambda)$ conducted with a HyperPro free-fall profiler (Satlantic, Inc.) adapted to float at the sea surface and deployed ~100 m from the ship. It is worth noting that their reflectance values, determined from subsurface measurements, were similar to ours, obtained from vertical profiles, in the domain 380–565 nm (Figure 3). *Morel et al.* [2007a, 2007b] and *Stramski et al.* [2008] found the highest reflectances around 395 nm. Hence, even though we observed in the SPG maximal $nL_w(\lambda)$ at 412 nm, spectral measurements prove that the highest values were actually located at the UV-visible boundary (~395 nm). Plotting $nL_w(\lambda)$ against the ratios $b_b(\lambda)/[a(\lambda) + b_b(\lambda)]$ gave linear relationships with r^2 ranging from 0.58 (490 nm) to 0.92 (325 nm) (Figure 4). These results confirm the strong influence of the backscattering/absorption coefficient ratio on water-leaving radiances in both UV and visible spectral domains.

[21] Values of $nL_w(\lambda)$ (or corresponding $R_{rs}(\lambda)$) in the violet-blue domains, determined in the SPG, are appreciably higher than those measured in other oligotrophic oceanic areas. For example, in the southwest Atlantic (10°S–30°S, 15°W–35°W), $nL_w(412)$, $nL_w(443)$, and $nL_w(490)$ reached up to 2.17, 1.78, and 1.31 μW cm^{-2} sr^{-1}, respectively, for Chl *a* concentrations of ~0.04 mg m^{-3} [*Garcia et al.*,

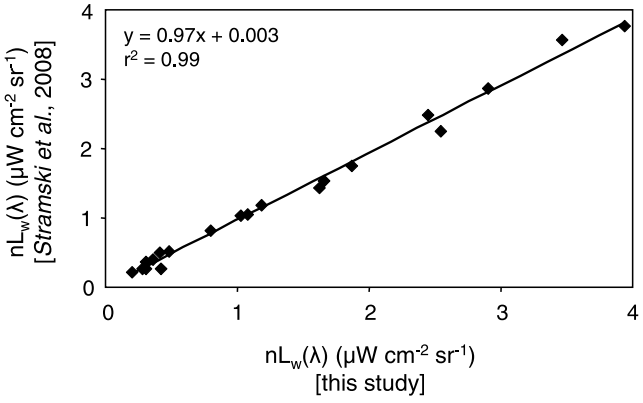

Figure 3. Comparison between normalized water-leaving radiance ($nL_w(\lambda)$) values obtained from two different in-water radiometric methods, i.e., free-fall profiling measurements of $L_u(Z, \lambda)$ by means of a Satlantic MicroPro profiler (this study) and subsurface measurements of $L_u(\lambda)$ with a Satlantic HyperPro profiler floating at the sea surface [*Stramski et al.*, 2008]. Both techniques used above-water measurements of irradiance ($E_d(0^+, \lambda)$). Values are reported for four stations (GYR, EGY5, STA21, and UPW1) and five wave bands (380, 412, 443, 490, and 565 nm), so the number of observations is 20. Measurements were made the same day with 1–3 h gap, except at GYR station, where they were performed at day 3 (GYR3 [*Stramski et al.*, 2008]) and day 5 (GYR5 (this study)). $R_{rs}(\lambda)$ data from *Stramski et al.* [2008] were converted into $nL_w(\lambda)$ by applying *Thuillier et al.*'s [1998] $F_0(\lambda)$ values.

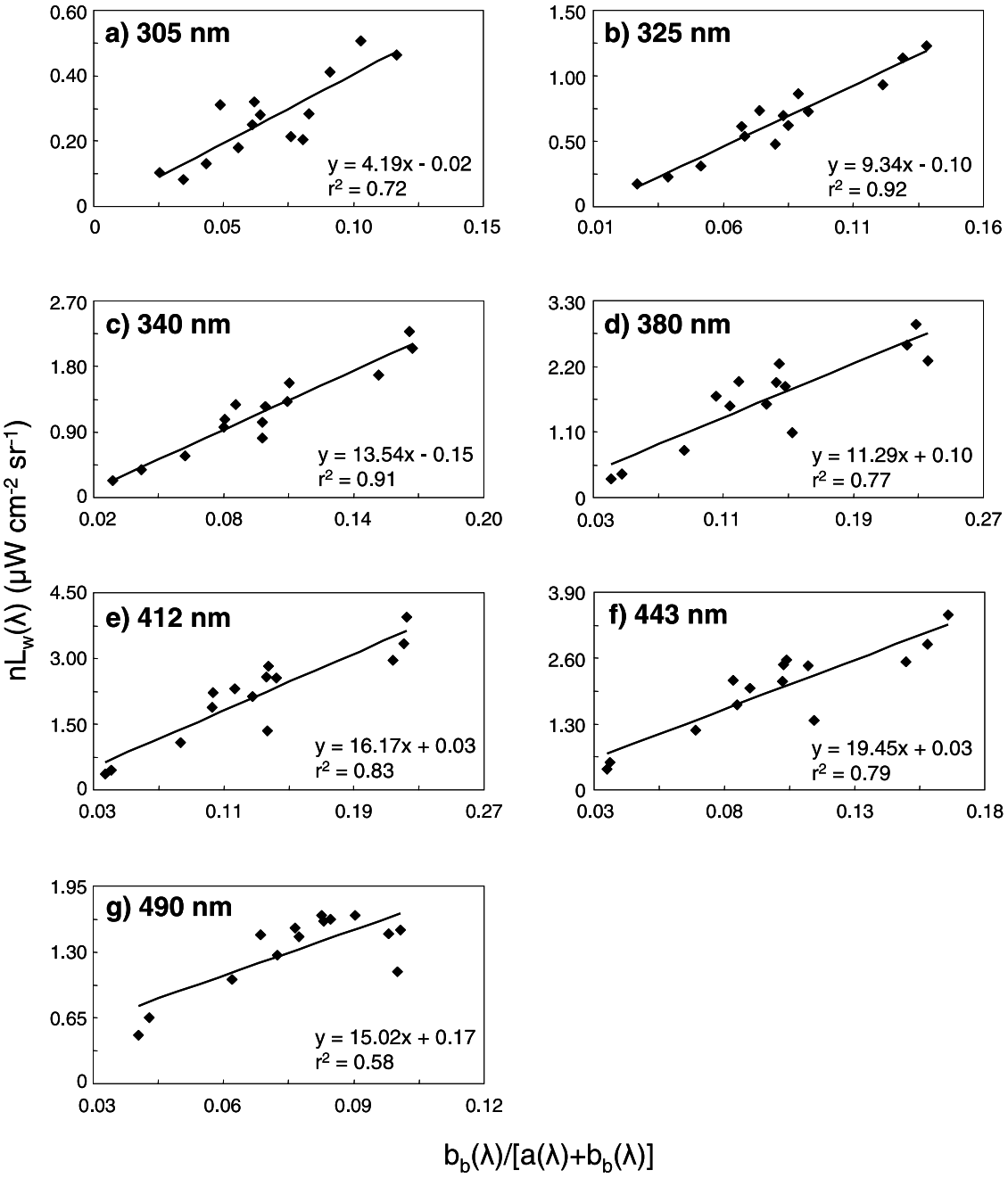

Figure 4. Linear relationship between the ratio of total backscattering coefficient to the sum of total absorption and backscattering coefficients, $b_b(\lambda)/[a(\lambda) + b_b(\lambda)]$, and normalized water-leaving radiance ($nL_w(\lambda)$). The wavelength λ is (a) 305, (b) 325, (c) 340, (d) 380, (e) 412, (f) 443, and (g) 490 nm. Total backscattering coefficient corresponds to the sum of backscattering coefficient of pure seawater ($b_{bsw}(\lambda)$), which was derived from scattering coefficient of pure seawater reported by *Morel et al.* [2007a] and backscattering coefficient of particles ($b_{bp}(\lambda)$) determined by *Huot et al.* [2008, equations 8, 8a, and 8b]. These equations were originally provided for the spectral domain 420–650 nm and were applied here to the range 305–490 nm. Total absorption coefficient corresponds to the sum of absorption coefficient of pure seawater ($a_{sw}(\lambda)$), obtained from *Morel et al.* [2007a], and absorption coefficients of phytoplankton ($a_{\mathrm{Phy}}(\lambda)$) of colored dissolved organic matter ($a_{\mathrm{CDOM}}(\lambda)$) and of nonalgal particulate matter ($a_{\mathrm{NAP}}(\lambda)$) (this study). The stations MAR2, STB6, STB11, STB12, STB18 (CDOM and NAP data not available), STB7, and STB20 ($nL_w(\lambda)$ data not available) are not reported. The number of observations is 14. All these linear relationships are significant (Fisher test: $p < 0.001$ or $p < 0.01$).

2005], which corresponds approximately to 49%, 45%, and 70% of our maximal values encountered in STB6. *Werdell and Bailey* [2005] presented $R_{rs}(\lambda)$ computed in the framework of the NASA bio-optical Marine Algorithm data set (NOMAD). This data set included over 3400 stations of various oceanic regions with Chl *a* concentrations ranging from 0.012 to 72 mg m^{-3}. Among the stations with Chl *a* concentrations <0.04 mg m^{-3} (which is roughly the range of TChl *a* found in the SPG), the highest $nL_w(412)$ and $nL_w(443)$ reported by these authors were 3.05 and 3.07 μW cm^{-2} sr^{-1}, respectively. Note that data were originally given in terms of $R_{rs}(\lambda)$ values by *Werdell and Bailey* [2005] and that we converted them into $nL_w(\lambda)$ by applying $F_0(\lambda)$ values by *Thuillier et al.* [1998]. Thus, these $nL_w(\lambda)$ values were substantially lower than those measured in the clearest stations of the SPG (corresponding to 68% and 78% of $nL_w(412)$ and $nL_w(443)$ in STB6, respectively), despite equivalent Chl *a* concentrations. Nonetheless, for the blue-green domain (490 nm), their values were analogous to ours (i.e., 1.85 μW cm^{-2} sr^{-1}). These comparisons highlight the specific character of the SPG with "excessive" (with regard to Chl *a* concentrations) water-leaving radiances in the violet-blue region. This "excess" of $nL_w(\lambda)$ in this hyper-oligotrophic area may be attributed to relatively low absorptions of violet and blue radiation by CDOM and particulate detritus as seen by $a_{CDM}(\lambda)$ values ($a_{CDM}(412)$ in the SPG: 0.0066–0.0068 m^{-1}). On the other hand, $nL_w(565)$ values obtained in the upwelling of Chile (0.36 and 0.42 μW cm^{-2} sr^{-1}) fell into the range reported by *Werdell and Bailey* [2005] for stations with Chl *a* concentrations between 0.64 and 1.28 mg m^{-3}.

[22] Concerning the UV domain, the comparison of $nL_w(\lambda)$ recorded in the southeast Pacific with other oceanic regimes is much more difficult because of a lack of data. This may be explained by the fact that the UV domain is not directly concerned by ocean color data that refer to visible wavelengths. Space sensors such as SeaWiFS, MODIS, and MERIS are not currently equipped for UV wave bands, and all the biogeochemical products (e.g., Chl *a*, POC, and CDM) derived from remote sensing measurements generally originate from algorithms based on blue/green wave band ratios. Moreover, nL_w(UV) and R_{rs}(UV) determined from in situ radiometric measurements are also rarely reported since $L_u(\lambda)$ sensors in the short UV wave bands (300–350 nm) are relatively new and not widespread yet. However, although the comparisons with nL_w(UV) data are not really possible, as the discrepancies observed in the violet-blue domains are likely due to the CDM content (both CDOM and NAP are characterized by increasing absorption values toward the UV domain [see *Bricaud et al.*, 1981; *Nelson et al.*, 1998]), nL_w(UV) values measured in the SPG are probably "excessive" compared to those that would be observed in other oligotrophic waters. These higher divergences in the UV region have been underlined by *Morel et al.* [2007a, 2007b] for $R(\lambda)$ and $K_d(\lambda)$ data.

3.4. Relationships Between $nL_w(\lambda)$ and TChl *a* Concentration/CDM Absorption

[23] We examined the power relationships between the UV, violet, or blue/green wave band ratios of $nL_w(\lambda)$ and surface TChl *a* concentration (Figure 5) and CDM absorption (Figure 6). The two upwelling stations (UPW1 and UPX2, eutrophic sites) were excluded from these relationships because their TChl *a* and CDM contents were high compared to those of other stations (oligotrophic and mesotrophic sites), leading to a strong increase in determination coefficients when all values were plotted together. In addition, stations MAR2, STB6, STB11, STB12, STB18 (CDOM and/or NAP measurements not available), STB7, and STB20 ($nL_w(\lambda)$ data not available) are not presented. For TChl *a* concentration, the correlations were significantly higher when using the violet-blue/green wave band ratios, i.e., 412, 443, or 490/565 nm (r^2 = 0.81–0.86 and RMSE = 23%–28% (Figures 5e–5g)) than the UV/green ones, i.e., 305, 325, 340, or 380/565 nm (r^2 = 0.55–0.81 and RMSE = 25%–36% (Figures 5a–5d)). The best correlation was found at 443 nm with TChl *a* (mg m^{-3}) = $2.37[nL_w(443)/nL_w(565)]^{-1.51}$ (r^2 = 0.86 and RMSE = 23% (Figure 5f)). In contrast, when considering $a_{CDM}(\lambda)$, the correlations were better with the UV/green wave band ratios (r^2 = 0.50–0.82 and RMSE = 16%–28% (Figures 6a–6d)) compared to the violet-blue/green ones (r^2 = 0.40–0.71 and RMSE = 29%–72% (Figures 6e–6g)), and the highest correlation was observed at 325 nm: $a_{CDM}(325)$ (m^{-1}) = $0.16[nL_w(325)/nL_w(565)]^{-0.69}$ (r^2 = 0.82 and RMSE = 16% (Figure 6b)).

[24] Phytoplankton, which strongly absorbs radiation in the blue and weakly in the green, usually displays an absorption spectrum with a maximum peak at 440 nm [*Kirk*, 1994, and references therein]. Hence, the spectral domain with the highest correlation between TChl *a* concentration and $nL_w(\lambda)$ (Figure 5f) corresponds with that for the maximum peak of phytoplankton absorption spectra, which is well known and not surprising. Nevertheless, for colored detrital matter, the correlations did not exactly follow CDOM and NAP absorption spectra, i.e., increasing absorption values in the direction of short wave bands. Indeed, at 305 nm, r^2 (0.50) was much lower than those reported for longer UV wave bands (0.67–0.82) (Figures 6a–6d). This unexpected weak correlation between $nL_w(305)$ and $a_{CDM}(305)$ could be intrinsically explained by the low amplitude of the $nL_w(305)/nL_w(565)$ ratio that ranged from 0.32 to 2.33 (Figure 6a). The use of $nL_w(305)$ and $nL_w(565)$, which are of the same order of magnitude (Figure 2), may not be suitable for assessing $a_{CDM}(305)$. The best compromise between high CDM absorption and high UV/green wave band ratio was found at 325 nm (highest r^2 (Figure 6b)). When examining the correlations between $nL_w(412)/nL_w(565)$ and $a_{CDM}(305)$, $a_{CDM}(325)$, $a_{CDM}(340)$, and $a_{CDM}(380)$, we found r^2 and RMSE of 0.63 and 21%, 0.77 and 18%, 0.76 and 20%, and 0.71 and 28%, respectively (figure not shown). Therefore, $a_{CDM}(305)$ was better correlated to $nL_w(412)/nL_w(565)$ than to $nL_w(305)/nL_w(565)$. This demonstrates that the latter is not suitable enough to assess CDM absorption at short UV wave bands. Assessing $a_{CDM}(\lambda)$ at longer UV wave bands (325, 340, and 380 nm) is overall slightly better when using the corresponding UV/green wave band ratio than the violet/green one.

[25] Table 3 presents the relative contribution of phytoplankton, CDOM, and NAP in the total light absorption in the surface waters. In the UV domain, colored detrital matter (CDOM + NAP) was the main contributor to light absorption, with, on average, 94%, 91%, 89%, and 88% at 305, 325, 340, and 380 nm, respectively. CDOM represented, on average, 94%, 93%, 91%, and 88% of this

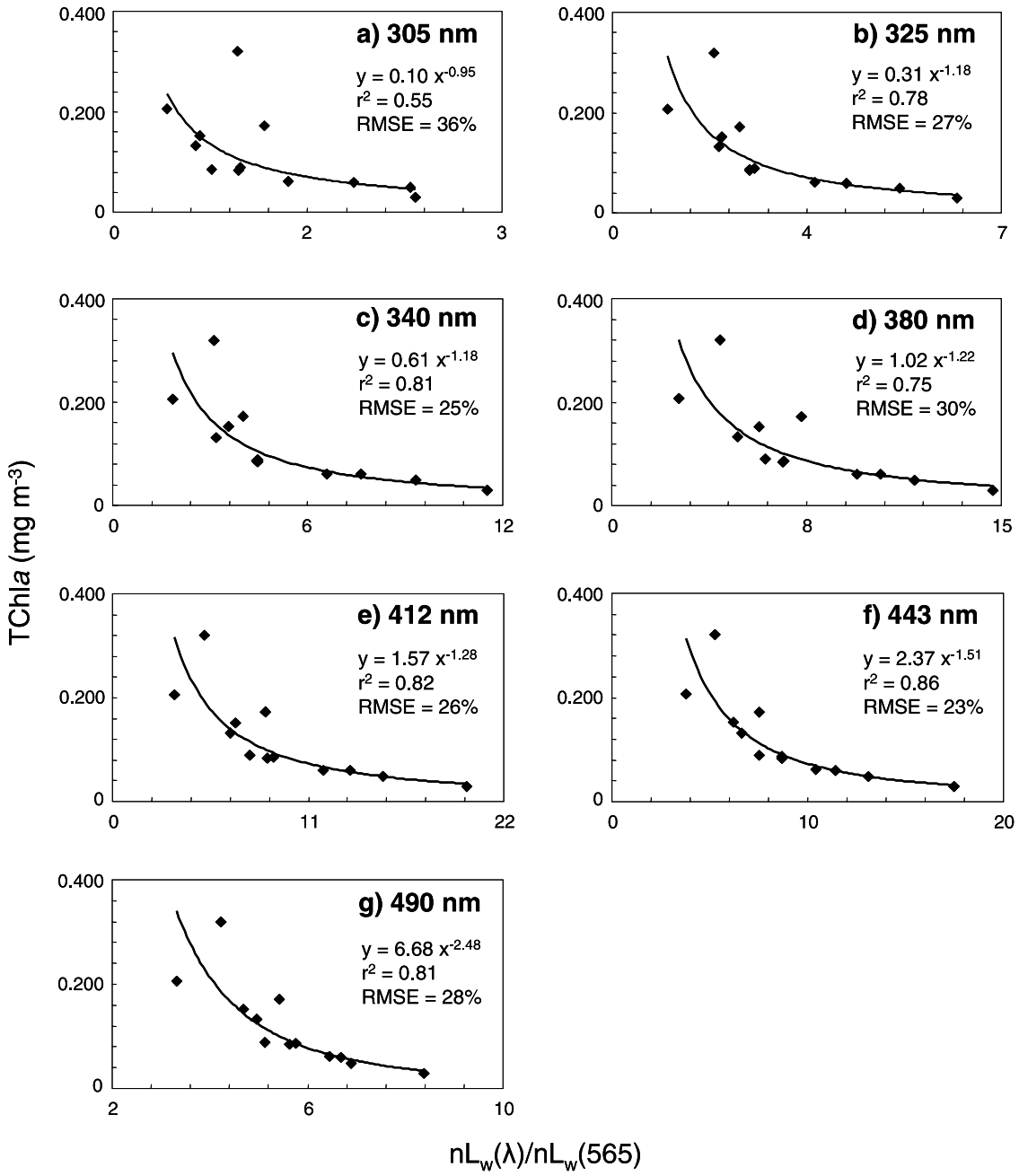

Figure 5. Relationship (power function) between the UV, violet, or blue/green wave band ratio of normalized water-leaving radiance ($nL_w(\lambda)/nL_w(565)$) and surface total chlorophyll *a* (TChl *a*) concentration. The wavelength λ is (a) 305, (b) 325, (c) 340, (d) 380, (e) 412, (f) 443, and (g) 490 nm. Relative root-mean-square error (RMSE) is calculated between retrieved and measured surface TChl *a* concentration values. The stations UPW1, UPX2 (TChl $a \geq 1$ mg m^{-3}), MAR2, STB6, STB11, STB12, STB18 (CDOM and NAP data not available), STB7, and STB20 ($nL_w(\lambda)$ data not available) are not reported. The number of observations is 12. All these power relationships are significant (Fisher test: $p < 0.001$ or $p < 0.01$).

colored material (Table 3). The contribution of phytoplankton in the UV region was low (on average 6%–12%), despite the presence in this area of the southeast Pacific of mycosporine-like amino acids (MAAs) [*Bricaud et al.*, 2010]. MAAs are UV-absorbing compounds produced by phytoplankton cells to prevent harmful solar UV radiation, which has been shown to reach significant depths and affect biogeochemical compartments in the southeast Pacific waters [*Morel et al.*, 2007a; *Tedetti et al.*, 2007; *Sempéré et al.*, 2008; *Van Wambeke et al.*, 2009]. Consequently, the distribution of $nL_w(\lambda)$ in the UV range was principally driven by CDM, without any or with only a very weak influence of phytoplankton (MAAs). In this sense, the slight differences observed between the correlations with TChl *a*

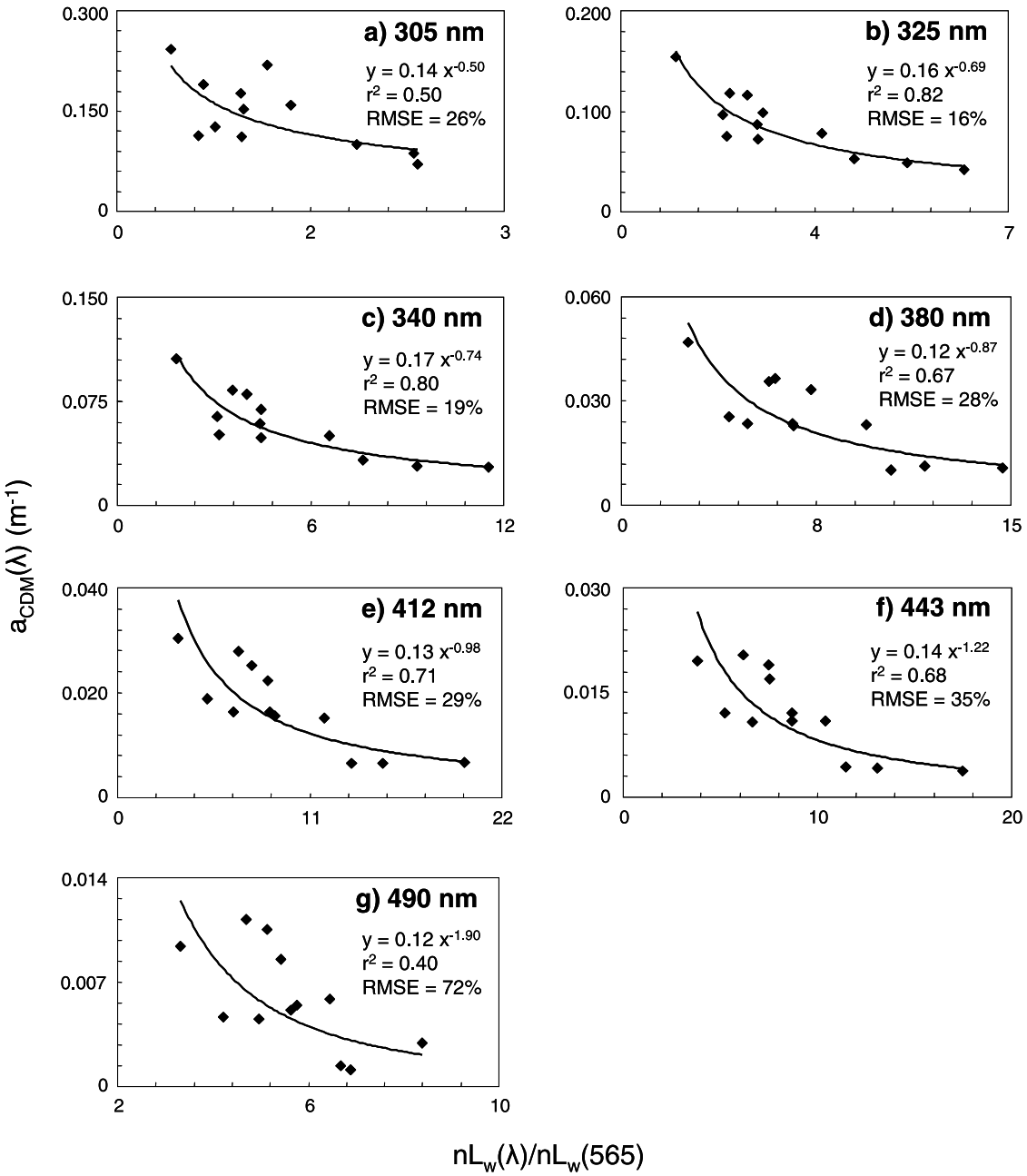

Figure 6. Relationship (power function) between the UV, violet, or blue/green wave band ratio of normalized water-leaving radiance ($nL_w(\lambda)/nL_w(565)$) and surface colored detrital material absorption ($a_{CDM}(\lambda)$). The wavelength λ is (a) 305, (b) 325, (c) 340, (d) 380, (e) 412, (f) 443, and (g) 490 nm. Relative RMSE is calculated between retrieved and measured surface $a_{CDM}(\lambda)$ values. The stations UPW1, UPX2 (TChl $a \geq 1$ mg m^{-3}), MAR2, STB6, STB11, STB12, STB18 (CDOM and NAP data not available), STB7, and STB20 ($nL_w(\lambda)$ data not available) are not reported. The number of observations is 12. All these power relationships are significant (Fisher test: $p < 0.001$ or $p < 0.05$).

(Figures 5a–5d) and those with a_{CDM}(UV) (Figures 6a–6d) reflected the degree of connection between these two biogeochemical parameters. Concerning the visible domain, CDM was still the highest contributor to light absorption at 412 and 443 nm, with, on average, 74% and 60%, respectively (Table 3). However, at 490 nm, absorptions by CDM and phytoplankton were of the same order of magnitude, with, on average, 51% and 49%, respectively. Because of their respective absorption spectrum, the contribution of phytoplankton in the total absorption (and thus in the $nL_w(\lambda)$ signal) was lower at 412 (26%) than at 443 nm (40%), whereas the inverse pattern was found for CDM. For the violet-blue wave bands, the fraction of CDOM in the CDM pool was slightly lower than for the UV wave bands, with, on average, 82%–87% (Table 3). Therefore, in contrast to nL_w(UV), the distribution of $nL_w(\lambda)$ in the visible region was controlled by both TChl *a* and CDM.

Table 3. Relative Contributions of Phytoplankton, Colored Dissolved Organic Matter, and Nonalgal Particulate Matter in the Total Absorption at Different UV and Visible Wave Bands in the Surface Waters[a]

	305 nm			325 nm			340 nm			380 nm			412 nm			443 nm			490 nm		
Station	Phy	CDOM	NAP	Phy	CDOM	NAP	Phy	CDOM	NAP	Phy	CDOM	NAP	Phy	CDOM	NAP	Phy	CDOM	NAP	Phy	CDOM	NAP
MAR4	4	92	4	10	84	6	12	81	7	11	77	12	26	64	10	44	48	9	58	32	10
HNL2	2	92	6	3	90	7	4	87	9	6	80	14	15	74	12	26	64	10	31	58	11
STB1	3	94	2	7	90	4	7	88	4	8	85	6	21	73	6	35	61	4	43	53	4
STB3	3	94	2	6	90	3	7	89	4	8	86	6	22	72	6	37	59	5	42	54	5
STB4	4	93	3	6	90	4	7	88	5	11	79	10	30	62	8	49	46	6	65	28	7
STB5	3	94	3	5	91	4	5	89	6	7	84	8	24	68	8	42	51	7	61	30	9
STB7	2	95	3	3	92	5	3	90	7	4	86	10	15	74	11	25	66	9	29	62	10
GYR5	5	92	4	7	89	5	8	86	6	6	84	11	16	73	10	32	57	11	27	64	9
EGY3	5	91	4	7	87	5	9	85	6	7	85	8	15	77	8	25	68	6	30	64	7
EGY4	6	88	7	10	81	8	13	77	10	10	76	14	21	67	13	33	57	11	44	43	13
EGY5	4	92	4	6	89	5	8	86	6	8	83	10	19	72	9	32	61	7	37	55	8
STB17	10	83	7	19	74	7	23	69	8	20	69	10	32	60	8	47	47	6	60	34	6
STB20	7	85	8	10	81	9	12	78	10	14	73	13	29	59	12	45	46	9	53	39	9
STA21	6	88	5	9	84	7	11	80	8	16	73	11	32	58	10	50	42	9	62	30	8
UPW1	19	71	9	27	63	10	30	60	10	31	56	13	48	42	10	62	29	9	72	20	8
UPX2	9	80	10	13	76	12	17	70	13	28	58	14	46	43	11	62	29	9	69	21	10

[a]Relative contributions in %. Phy, phytoplankton; CDOM, colored dissolved organic matter; NAP, nonalgal particulate matter. Data were not available for stations MAR2, STB6, STB11, STB12, and STB18.

[26] *Morel et al.* [2007b] already pointed out that the CDOM pool, which represents the major fraction of CDM [*Siegel et al.*, 2002], and phytoplankton biomass were less connected in the southeast Pacific (even though a significant linear relationship was found between $a_{CDOM}(370)$ and TChl *a* [e.g., *Morel et al.*, 2007a]) than in the Mediterranean Sea. This "relative" disconnection may be attributed to different factors controlling the abundance and distribution of these parameters. In the surface waters of open oceans, CDOM content is strongly regulated by photobleaching that corresponds to the loss of absorption and fluorescence properties caused by its photochemical degradation [*Nelson and Siegel*, 2002; *Coble*, 2007]. Photobleaching, which has been proposed to be significant in the southeast Pacific because of high levels of incident solar radiation [*Morel et al.*, 2007b; *Tedetti et al.*, 2007; *Sempéré et al.*, 2008], could play a significant role in this "relative" decoupling between TChl *a* and colored material and in the distribution of $nL_w(\lambda)$ observed.

4. Conclusion

[27] In the present work, we show the specific bio-optical character of the South Pacific Gyre through the distribution of $nL_w(\lambda)$ in the visible and UV domains. Values of $nL_w(\lambda)$ of the violet-blue regions are described as "excessive" because they are significantly higher than those reported for other oligotrophic oceanic areas that present the same (very low) surface TChl *a* concentrations [*Werdell and Bailey*, 2005]. These "excessive" values have been also reported by *Morel et al.* [2007b] for $R(\lambda)$ and $K_d(\lambda)$ data and could be associated with a relatively low CDM content (with regard to TChl *a* concentration) due to a strong photobleaching of CDOM occurring in the surface waters of the South Pacific Gyre. In addition, we assess in this study the spectral (UV-visible) discrimination between TChl *a* and CDM in their linkage with $nL_w(\lambda)$. While the high correlation between TChl *a* concentration and $nL_w(443)/nL_w(565)$ was expected, for CDM, we found the highest correlation with $nL_w(325)/nL_w(565)$. Methods that used $nL_w(443)$ measurements to derive $a_{CDM}(443)$ have to take into account a possible "pollution" by the Chl *a* signal (and vice versa) due to the overlap in their absorption spectrum [*Siegel et al.*, 2002; *Maritorena and Siegel*, 2005]. Therefore, the use of the $nL_w(325)/nL_w(565)$ wave band ratio, which depends exclusively on the CDM content (even with the presence of MAAs within the phytoplankton community), could be very helpful for the direct evaluation of $a_{CDM}(325)$. For example, *Hooker et al.* [2007] underscored the potential use of UV wave bands on space radiometers, first to improve atmospheric correction algorithms in the presence of absorbing aerosols and second to distinguish the absorption signals of Chl *a* and CDM. Moreover, the direct estimate of $a_{CDM}(\lambda)$ at several UV wave bands from $nL_w(UV)/nL_w(565)$ may be relevant to provide a real appraisal of absorption spectral slope coefficients over the UV domain, which could bring substantial information about the nature of CDM. Undoubtedly, our conclusions are based on a limited number of samples, and additional measurements of $nL_w(UV)$ along with $a_{CDOM}(UV)$ and $a_{NAP}(UV)$ in other oceanic provinces are required in order to improve these relationships.

[28] **Acknowledgments.** We are grateful to the captain and crew of the R/V *l'Atalante* for excellent service during the BIOSOPE campaign. We acknowledge H. Claustre as the leader of the BIOSOPE project and chief scientist of the first leg of the cruise and A. Sciandra as the chief scientist of the second leg. We warmly thank C. Bournot, D. Tailliez, and D. Merien for CTD-rosette operations and data processing, as well as F. Tièche for her help with CDOM analyses. We express gratitude to M. Babin for NAP analyses and for his constructive comments on this manuscript. M. Lewis, N. Souaidia, A. Morel, and S. Hooker are acknowledged for their assistance during the radiometric measurements. We also thank A. Vasilkov for valuable discussions as well as two anonymous reviewers for improving the quality of this manuscript. This research was funded by CNRS LEFE-CYBER programs BIOSOPE and UVECO and the region of Provence Alpes Côte d'Azur.

References

Allali, K., A. Bricaud, and H. Claustre (1997), Spatial variations in the chlorophyll-specific absorption coefficients of phytoplankton and photosynthetically active pigments in the equatorial Pacific, *J. Geophys. Res.*, *102*, 12,413–12,423, doi:10.1029/97JC00380.

Blain, S., S. Bonnet, and C. Guieu (2008), Dissolved iron distribution in the tropical and sub tropical south eastern Pacific, *Biogeosciences*, *5*, 269–280.

Bricaud, A., and D. Stramski (1990), Spectral absorption coefficients of living phytoplankton and nonalgal biogenous matter: A comparison between the Peru upwelling area and the Sargasso Sea, *Limnol. Oceanogr.*, *35*, 562–582.

Bricaud, A., A. Morel, and L. Prieur (1981), Absorption by dissolved organic matter in the sea (yellow substance) in the UV and visible domains, *Limnol. Oceanogr.*, *28*, 43–53.

Bricaud, A., M. Babin, H. Claustre, J. Ras, and F. Tieche (2010), Light absorption properties and absorption budget of South Pacific waters, *J. Geophys. Res.*, doi:10.1029/2009JC005517, in press.

Carr, M. E. (2001), Estimation of potential productivity in eastern boundary currents using remote sensing, *Deep Sea Res., Part II*, *49*, 59–80, doi:10.1016/S0967-0645(01)00094-7.

Ciotti, A. M., and A. Bricaud (2006), Retrievals of a size parameter for phytoplankton and spectral light absorption by colored detrital matter from water-leaving radiances at SeaWiFS channels in a continental shelf region off Brazil, *Limnol. Oceanogr. Methods*, *4*, 237–253.

Claustre, H., and S. Maritorena (2003), The many shades of ocean blue, *Science*, *302*, 1514–1515, doi:10.1126/science.1092704.

Claustre, H., A. Sciandra, and D. Vaulot (2008), Introduction to the special section bio-optical and biogeochemical conditions in the southeast Pacific in late 2004: The BIOSOPE program, *Biogeosciences*, *5*, 679–691.

Coble, P. G. (2007), Marine optical biogeochemistry—The chemistry of ocean color, *Chem. Rev.*, *107*, 402–418, doi:10.1021/cr050350+.

D'Ortenzio, F., S. Marullo, M. Ragni, M. Ribera d'Alcalà, and R. Santoleri (2002), Validation of empirical SeaWiFS algorithms for chlorophyll *a* retrieval in the Mediterranean Sea: A case study for oligotrophic seas, *Remote Sens. Environ.*, *82*, 79–94, doi:10.1016/S0034-4257(02)00026-3.

Garcia, C. A. E., V. M. T. Garcia, and C. R. McClain (2005), Evaluation of SeaWiFS chlorophyll algorithms in the southwestern Atlantic and Southern oceans, *Remote Sens. Environ.*, *95*, 125–137, doi:10.1016/j.rse.2004.12.006.

Gordon, H. R. (2005), Normalized water-leaving radiance: Revisiting the influence of surface roughness, *Appl. Opt.*, *44*, 241–248, doi:10.1364/AO.44.000241.

Gordon, H. R., and D. K. Clark (1981), Clear water radiances for atmospheric correction of Coastal Zone Color Scanner imagery, *Appl. Opt.*, *20*, 4175–4180, doi:10.1364/AO.20.004175.

Gordon, H. R., O. Brown, R. Evans, J. Brown, R. Smith, K. Baker, and D. Clark (1988), A semi-analytical radiance model of ocean color, *J. Geophys. Res.*, *93*, 10,909–10,924, doi:10.1029/JD093iD09p10909.

Hooker, S. B., C. R. McClain, and A. Mannino (2007), NASA strategic planning document: A comprehensive plan for the long-term calibration and validation of oceanic biogeochemical satellite data, *NASA Spec. Publ., SP-2007-214152*, 1–31.

Huot, Y., A. Morel, M. S. Twardowski, D. Stramski, and R. A. Reynolds (2008), Particle optical backscattering along a chlorophyll gradient in the upper layer of the eastern South Pacific Ocean, *Biogeosciences*, *5*, 495–507.

Kirk, J. (1994), *Light and Photosynthesis in Aquatic Ecosystems*, 2nd ed., 509 pp., Cambridge Univ. Press, Cambridge, U. K.

Kishino, M., M. Takzhashi, N. Okami, and S. Ichimura (1985), Estimation of the spectral absorption coefficients of phytoplankton in the sea, *Bull. Mar. Sci.*, *37*, 634–642.

Maritorena, S., and D. A. Siegel (2005), Consistent merging of satellite ocean color data sets using a bio-optical model, *Remote Sens. Environ.*, *94*, 429–440, doi:10.1016/j.rse.2004.08.014.

Morel, A., and L. Prieur (1977), Analysis of variations in ocean color, *Limnol. Oceanogr.*, *22*, 709–722.

Morel, A., B. Gentili, H. Claustre, M. Babin, A. Bricaud, J. Ras, and F. Tieche (2007a), Optical properties of the "clearest" natural waters, *Limnol. Oceanogr.*, *52*, 217–229.

Morel, A., H. Claustre, D. Antoine, and B. Gentili (2007b), Natural variability of bio-optical properties in case 1 waters: Attenuation and reflectance within the visible and near-UV spectral domains, as observed in South Pacific and Mediterranean waters, *Biogeosciences*, *4*, 913–925.

Mueller, J. L., et al. (2003), Ocean optics protocols for satellite ocean color sensor validation, in *Radiometric Measurements and Data Analysis Protocols*, vol. 3, 4th rev., edited by J. L. Mueller, G. S. Fargion, and C. R. McClain, *NASA Tech. Memo., TM-2003-211621*, 1–78.

Nelson, N. B., and D. A. Siegel (2002), Chromophoric DOM in the open ocean, in *Biogeochemistry of Marine Dissolved Organic Matter*, edited by D. A. Hansell and C. A. Carlson, pp. 547–578, Academic, San Diego, Calif.

Nelson, N. B., D. A. Siegel, and A. F. Michaels (1998), Seasonal dynamics of colored dissolved material in the Sargasso Sea, *Deep Sea Res., Part I*, *45*, 931–957, doi:10.1016/S0967-0637(97)00106-4.

O'Reilly, J. E., et al. (2000), Ocean color chlorophyll *a* algorithms for SeaWiFS, OC2, and OC4: Version 4, in *SeaWiFS Postlaunch Calibration and Validation Analyses, Part 3*, *SeaWiFS Postlaunch Tech. Rep. Ser.*, vol. 11, edited by S. B. Hooker and E. R. Firestone, *NASA Tech. Memo., TM-2000-206892*, 9–27.

Pabi, S., and K. R. Arrigo (2006), Satellite estimation of marine particulate carbon in waters dominated by different phytoplankton taxa, *J. Geophys. Res.*, *110*, C09003, doi:10.1029/2005JC003137.

Preisendorfer, R. W. (1961), *Application of Radiative Transfer Theory to Light Measurements in the Sea*, *IUGG Monogr.*, vol. 10, pp. 11–30, Int. Union of Geod. and Geophys., Karlsruhe, Germany.

Raimbault, P., J. Neveux, and F. Lantoine (2004), Dosage rapide de la chlorophylle a et des phaeopigments a par fluorimétrie après extraction au méthanol. Comparaison avec la méthode classique d'extraction à l'acétone, *Oceanis*, *30*, 189–205.

Raimbault, P., N. Garcia, and F. Cerrutti (2008), Distribution of inorganic and organic nutrients in the South Pacific Ocean—Evidence for long-term accumulation of organic matter in nitrogen-depleted waters, *Biogeosciences*, *5*, 281–298.

Ras, J., H. Claustre, and J. Uitz (2008), Spatial variability of phytoplankton pigment distributions in the subtropical South Pacific Ocean: Comparison between in situ and predicted data, *Biogeosciences*, *5*, 353–369.

Sempéré, R., M. Tedetti, C. Panagiotopoulos, B. Charrière, and F. Van Wambeke (2008), Distribution and bacterial availability of dissolved neutral sugars in the southeast Pacific, *Biogeosciences*, *5*, 1165–1173.

Siegel, D. A., S. Maritorena, N. B. Nelson, D. A. Hansell, and M. Lorenzi-Kayser (2002), Global distribution and dynamics of colored dissolved and detrital organic materials, *J. Geophys. Res.*, *107*(C12), 3228, doi:10.1029/2001JC000965.

Signorini, S. R., C. R. McClain, and Y. Dandonneau (1999), Mixing and phytoplankton bloom in the wake of Marquesas Islands, *Geophys. Res. Lett.*, *26*, 3121–3214, doi:10.1029/1999GL010470.

Stramski, D., R. A. Reynolds, M. Kahru, and B. G. Mitchell (1999), Estimation of particulate organic carbon in the ocean from satellite remote sensing, *Science*, *285*, 239–242, doi:10.1126/science.285.5425.239.

Stramski, D., et al. (2008), Relationships between the surface concentration of particulate organic carbon and optical properties in the eastern South Pacific and eastern Atlantic oceans, *Biogeosciences*, *5*, 171–201.

Tedetti, M., R. Sempéré, A. Vasilkov, B. Charrière, D. Nérini, W. L. Miller, K. Kawamura, and P. Raimbault (2007), High penetration of ultraviolet radiation in the southeast Pacific waters, *Geophys. Res. Lett.*, *34*, L12610, doi:10.1029/2007GL029823.

Thuillier, G., M. Hersé, P. C. Simon, D. Labs, H. Mandel, and D. Gillotay (1997), Observation of the UV solar spectral irradiance between 200 and 350 nm during the ATLAS 1 mission by the SOLSPEC spectrometer, *Sol. Phys.*, *171*, 283–302, doi:10.1023/A:1004930219506.

Thuillier, G., M. Hersé, P. C. Simon, D. Labs, H. Mandel, D. Gillotay, and T. Foujols (1998), The visible solar spectral irradiance from 350 nm to 850 nm as measured by the SOLSPEC spectrometer during the ATLAS 1 mission, *Sol. Phys.*, *177*, 41–61, doi:10.1023/A:1004953215589.

Twardowski, M. S., H. Claustre, S. A. Freeman, D. Stramski, and Y. Huot (2007), Optical backscattering properties of the "clearest" natural waters, *Biogeosciences*, *4*, 1041–1058.

Uitz, J., H. Claustre, A. Morel, and S. Hooker (2006), Vertical distribution of phytoplankton communities in open ocean: An assessment based on surface chlorophyll, *J. Geophys. Res.*, *111*, C08005, doi:10.1029/2005JC003207.

Van Wambeke, F., M. Tedetti, S. Duhamel, and R. Sempéré (2009), Diel variability of heterotrophic bacterial production and underwater UV doses in the eastern South Pacific, *Mar. Ecol. Prog. Ser.*, *387*, 97–108, doi:10.3354/meps08075.

Welschmeyer, N. A. (1994), Fluorometric analysis of chlorophyll *a* in the presence of chlorophyll *b* and pheopigments, *Limnol. Oceanogr.*, *39*, 1985–1992.

Werdell, P. J., and S. W. Bailey (2005), An improved in situ bio-optical data set for ocean color algorithm development and satellite data product validation, *Remote Sens. Environ.*, *98*, 122–140, doi:10.1016/j.rse.2005.07.001.

A. Bricaud, Laboratoire d'Océanographie de Villefranche, Université Pierre et Marie Curie-Paris 6, INSU, CNRS, BP 8, F-06230 Villefranche-sur-Mer CEDEX, France.

B. Charrière, J. Para, P. Raimbault, R. Sempéré, and M. Tedetti, Laboratoire de Microbiologie, Géochimie et Ecologie Marines, Centre d'Océanologie de Marseille, Université de la Méditerranée, INSU, CNRS, Case 901, F-13288 Marseille CEDEX 9, France. (marc.tedetti@univmed.fr)